12th National Conference on Earthquake Engineering
Salt Lake City, Utah
27 June - 1 July 2022
Hosted by the Earthquake Engineering Research Institute

Fragility Analysis of Deteriorating Bridge Components Subjected to Simulated Ground-Motion Sequences

K. Otárola[1], J. Fayaz[2] and C. Galasso[3]

ABSTRACT

This study assesses the impact of corrosion deterioration on the seismic performance of bridge components during a sequence of ground motions. Specifically, a simplified methodology is proposed to derive state-dependent fragility relationships for bridge components (i.e., relationships that explicitly depend on the damage state achieved by the component during a first shock) subjected to chloride-induced corrosion deterioration and simulated ground-motion sequences. Specifically, vector-valued probabilistic seismic demand models are derived for various corrosion levels. Those models relate the dissipated hysteretic energy in the sequence to a deformation-based engineering demand parameter induced by the first shock and a ground-motion intensity measure of the second shock, calibrated *via* sequential cloud-based time-history analyses. For each corrosion level, fragility relationships are first derived for a single ground motion; state-dependent fragility relationships are then derived by considering the additional damage induced by a second ground motion within the simulated sequence (structure-specific damage states are considered). Finally, continuous functional models are developed from the analysis results to assemble fragility relationships at a given corrosion level. The results demonstrate the significant impact of environmental deterioration in seismic-prone regions, emphasising the necessity of accounting for deteriorating effects in current practice.

Introduction

Earthquake-induced ground motions lead to intermittent shocks to a structure during its lifetime, while ageing and deteriorating effects constitute a continuous mechanism of environmentally-induced damage accumulation [1]. Currently, it is known that a considerable proportion of the civil infrastructure systems/infrastructure components across the globe show visible signs of ageing and deterioration, especially near the end of their design lifetime [2]. Therefore, the simultaneous consideration of infrequent ground-motion sequences and ageing and deteriorating effects in seismic-prone regions is critical for risk preparedness and risk-informed decision making. Among the various mechanisms that structures are likely to experience when exposed to environmental hazards, chloride-induced corrosion deterioration is of particular interest from the structural performance standpoint [3]. The significance of considering primary and secondary effects of chloride-induced corrosion deterioration on structural material properties (e.g., area loss of steel rebar) for lifetime structural response and damage/loss has been addressed by several authors [4–6], emphasising the potential underestimation of seismic fragility/losses when not accounting for this threat [7–10]. Depending on the

[1] PhD student, Dept. of Science, Technology and Society, Scuola Universitaria Superiore (IUSS) Pavia, Pavia, PV 27100 (email: kenneth.otarola@iusspavia.it)
[2] Research fellow, Dept. of Civil, Environmental and Geomatic Engineering, University College London, London, WC1E 6BT
[3] Full professor, Dept. of Civil, Environmental and Geomatic Engineering, University College London, London, WC1E 6BT

Otárola K, Fayaz J, Galasso C. Fragility analysis of deteriorating bridge components subjected to simulated ground-motion sequences. *Proceedings of the 12th National Conference in Earthquake Engineering*, Earthquake Engineering Research Institute, Salt Lake City, UT. 2022.

severity of the environmental exposure, these mechanisms may lead to loss of structural capacity of structural components [11–13]. Therefore, efforts towards a structural performance-based assessment framework under joint seismic and environmental hazards are imperative. Here, a simplified methodology is presented to derive state-dependent fragility relationships for bridge components impacted by mainshock-induced ground-motion sequences for a chloride-induced corrosion deterioration level of interest. In the context of this paper, state-dependent fragility relationships explicitly express the dependency on the damage state achieved by a bridge component during a first shock. Specifically, the proposed methodology is exercised using the hybrid simulated ground motions from Cybershake 15.12 and a real ordinary bridge structure designed for southern California (La Veta Avenue, Orange, California). The assembled ground-motion sequences are utilised to perform nonlinear time-history analyses of the case-study bridge structure. The results of the analyses are then used to derive structure-specific fragility relationships for different corrosion levels under a single ground motion and state-dependent fragility relationships to model the increased damage caused by the following ground motion in the sequence. The results emphasise the necessity to incorporate deteriorating effects in risk assessment practice to account for the accelerated deterioration of structures during their lifetime.

State-dependent Fragility Analysis

A symmetric double-span box-girder seat-type bridge (denoted as bridge B in [14]) is selected as a study case to investigate the effects of the seismic sequences on the fragility of deteriorating structural components. The structural performance of ordinary bridge structures is mainly inferred by the response of their columns [15,16]. Therefore, in this study, the assessment is conducted primarily on the columns of the bridge's sole bent. The proposed state-dependent fragility relationships are not explicitly conditioned on time; instead, they are conditioned on a corrosion deterioration parameter (ψ) that implicitly depends on time [3]. In this study, ψ corresponds to the steel-rebar area-loss percentage [17], denominated arbitrarily as corrosion deterioration level. The corrosion deterioration level depends directly on the type of environmental exposure. Therefore, unlike exposure-specific time-dependent fragility relationships, the herein developed fragility relationships dependent on ψ are more applicable and generic for different exposure scenarios. In total, six equally spaced corrosion deterioration levels are considered ranging from 0% (i.e., pristine condition) up to 25%. Along with the area loss of rebar steel, corrosion deterioration results in various secondary effects. These secondary effects are accounted for in terms of reductions in structural material properties such as cover concrete strength [18], core concrete strength [19], steel yield strength [20], steel ultimate strength [20], and steel ultimate strain [21]; all been reduced as a function of ψ. For each corrosion deterioration level, a bridge computational model is developed; the adopted nonlinear modelling strategy implemented *via* the software framework OpenSeesPy [22] is consistent with the work of Fayaz et al. [15].

Monte-Carlo simulation is used to obtain catalogues (with interarrival times following the Poisson assumption) of simulated ground motions (hybrid simulations) from the CyberShake 15.12 [23,24] database, representing a 100-year bridge lifetime. In this study, among the ~900 southern California sites available in CyberShake [22], the simulations are obtained for Los Angeles Downtown (LADT) because of its proximity to seismic sources coupled with a large inventory of buildings and bridge structures. The simulated ground motion set is limited to the seismic sources [22] that lie within 100 km from the LADT site. The simulated ground motions for LADT are randomly sampled within this setting using the annual probabilities of occurrence of the corresponding rupture variations, ruptures and sources [23,24]. Ground-motion sequences are then assembled using consecutive simulated ground motions with a maximum interarrival time of 12 months between the events. This assumption is to select seismic sequences occurring between the probable decision/repairing actions after a significant earthquake event [9]. Finally, the 500 ground-motion sequences (i.e., a first mainshock, $GM1$, followed by a second mainshock, $GM2$) with higher $RotD50avgSA$ (denoted herein as $avgSA$ for brevity) in both shocks are arbitrarily selected (with a minimum threshold of 0.1g). The previous intensity measure (IM) is estimated as the geometrical mean of seven equally-spaced $RotD50$ pseudo-acceleration spectral ordinates [25] within the range $[T_3, 2.5T_3]$ including the fundamental structural

period, where T_3 (i.e., 0.37 s) is the dominant structural period in the transversal direction [26]. Note that the first three modal periods of the bridge structure are 0.83 s, 0.44 s and 0.37 s, respectively.

Sequential cloud-based nonlinear time-history analyses are performed using the above inputs for the various corrosion deterioration levels. For each considered ground-motion sequence, an analysis is conducted by rotating the two orthogonal components of the ground motions on the bridge structure through 180 degrees at 30 degrees intervals. From the obtained responses, the median value of the maximum curvature ($Rot50\phi$), as well as the column associated median of the dissipated hysteretic energy ($Rot50E_H$) are attained for both $GM1$ and $GM2$, respectively. This data is used to calibrate probabilistic seismic demand models ($PSDM$s), represented by a surface depending on the deformation-based engineering demand parameter (EDP) from the $GM1$ and the selected intensity measure (IM) from the $GM2$. The $PSDM$s are derived by fitting the response surface $E_{H,GM1GM2}(\phi_{GM1}, IM_{GM2})$ as per Gentile and Galasso [27]. $E_{H,GM1GM2}$ is the total dissipated hysteretic energy in the sequence (i.e., in $GM1$ and $GM2$; that is the summation of $Rot50E_H$); $E_{H,GM1}$ is the dissipated hysteretic energy during $GM1$ (i.e., $Rot50E_H$ due to $GM1$); $E_{H,GM2}$ is the dissipated hysteretic energy during $GM2$ (i.e., $Rot50E_H$ due to $GM2$); ϕ_{GM1} is the associated deformation-based EDP for $GM1$ ($Rot50\phi$); and IM_{GM2} is the associated IM for $GM2$ ($avgSA$). A five parameter (i.e., a, b, c, d, and m) functional form is fitted as shown in Eq. 1 for each corrosion deterioration level of the analysed structural component (i.e., the bridge column). The first term of Eq. 1 (i.e., ${a\phi_{GM1}}^b$) is practically described with a bilinear model, fitted using linear splines (i.e., continuous piecewise polynomials) in log-log space. The cloud data is partitioned into two discrete groups divided by breakpoints, where a first-order polynomial describes each group. The second term of Eq. 1 (i.e., ${c(1-m\phi_{GM1})IM_{GM2}}^d$) is fitted as per Gentile and Galasso [27].

$$E_{H,GM1GM2} = E_{H,GM1} + E_{H,GM2} = {a\phi_{GM1}}^b + {c(1-m\phi_{GM1})IM_{GM2}}^d \quad (1)$$

Using the deformation-based DS thresholds ($\overline{\phi_{DS}}$) for $GM1$ (estimated *via* pushover analyses) and the energy-based DS threshold ($\overline{E_{H,DS}}$) for $GM2$ (estimated with the $PSDM$s), and inverting Eq. 1, the median and dispersion of the desired fragility relationship are computed. A total of four DS are selected to perform the state-dependent fragility analyses, which are associated with: a) slight damage ($DS1$): steel rebar yielding strain; b) moderate damage ($DS2$): concrete cover extreme fibre ultimate strain; c) extensive damage ($DS3$): geometrical mean of $DS2$ and $DS4$; d) complete damage ($DS4$): concrete core extreme fibre or steel rebar ultimate strain. No damage is subsequently defined as $DS0$. Finally, continuous functional models are fitted using the previously obtained results using a polynomial quadratic functional form to predict the fragility median and dispersion at any corrosion deterioration level of interest.

Results

The developed continuous functional models and the derived fragility relationships are first presented for the component in pristine conditions to display the influence of the chloride-induced corrosion deterioration. After performing a stepwise regression, a polynomial quadratic functional form is selected for the fragility median and dispersion prediction models (Fig. 1a). The fitted models explain a high proportion of the variance (above 95% in every case). It can be observed that the deteriorating effects are more apparent at $DS4$, with a difference in the fragility median of the model of ~30% between the pristine and deteriorated (ψ =25%) conditions. It is also noticeable that the impact of corrosion on $DS1$ and $DS2$ are negligible for engineering purposes. This is more easily observable in the fragility relationships (Fig. 1b), where the fragility relationships correspondent to $DS3$ and $DS4$ are more apparently affected by the deterioration mechanism.

Similarly, to understand the combined effects of ground-motion sequences and corrosion deterioration effects, state-dependent fragility relationships are shown for pristine (Fig. 2a) and deteriorated (ψ =25%) (Fig. 2b) conditions. As expected, the difference in fragility median values indicates that the deteriorated component is more fragile than the pristine component. Moreover, exacerbated reductions in the fragility median values

are attained when conditioning on the various DSs, in the deteriorated component. For instance, differences up to ~12% are observed in the component in pristine conditions between $DS4|DS0$ and $DS4|DS3$ fragility median. On the other hand, differences up to ~32% are observed in the component in deteriorated (ψ =25%) conditions between $DS4|DS0$ and $DS4|DS3$ fragility median. In general, the fragility median values reduce as the corrosion deterioration level increases, and the differences between the undamaged and the damaged (conditioned on a previous DS) fragility median values are higher in a deteriorated component rather than one in pristine conditions, given a ground-motion sequence.

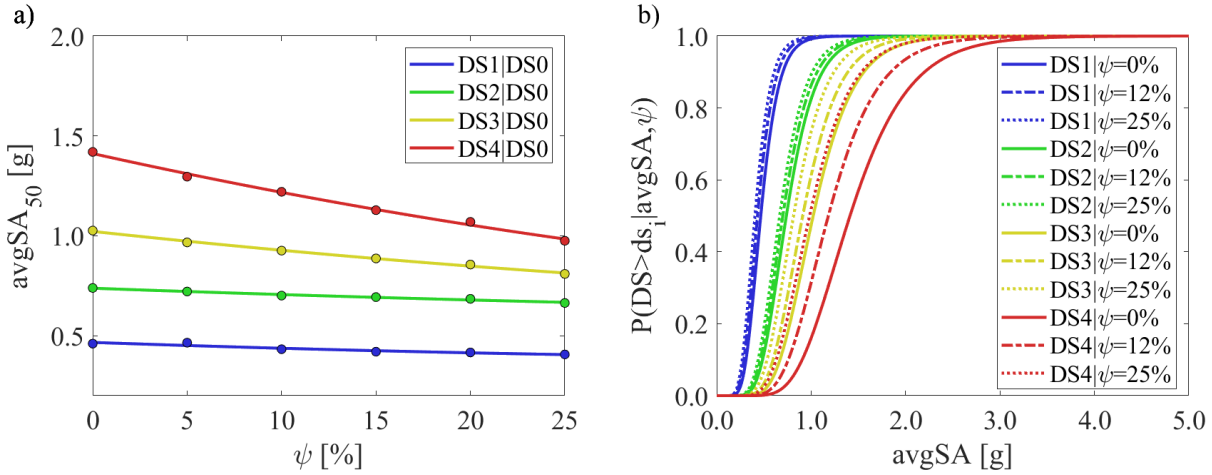

Figure 1. a) Fragility median values as a function of the ψ levels; and b) fragility relationships under various (i.e., 0%, 12% and 25%) ψ levels; of the bridge column.

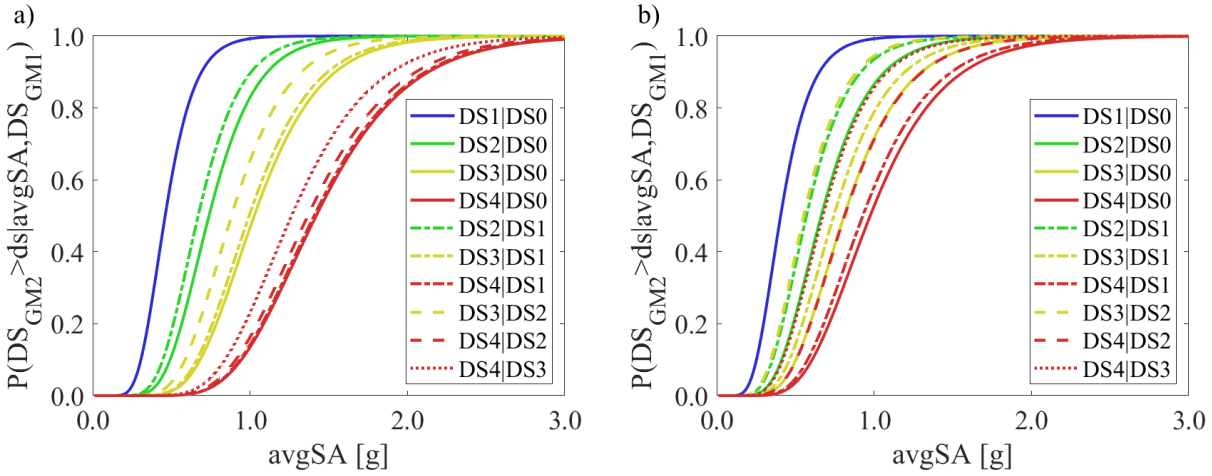

Figure 2. a) State-dependent fragility relationships in pristine condition (i.e., ψ=0%); and b) state-dependent fragility relationships in deteriorated (ψ=25%) condition; of the bridge column.

Conclusions

A simplified methodology to derive state-dependent fragility relationships for structural bridge components subjected to mainshock-induced ground-motion sequences while experiencing chloride-induced corrosion deterioration along their lifetime was presented. It was demonstrated that seismic and environmental multi-hazard mechanisms could negatively impact the fragility of structural components. It was further observed that the components become weaker following earthquake-induced damage, and corrosion-induced deterioration can accelerate this loss of structural capacity. Therefore, the combined consideration of infrequent ground-motion sequences and corrosion deterioration effects in seismic-prone regions is critical for risk preparedness and decision making to minimise societal losses.

References

1. Panchireddi B, Ghosh J. Cumulative vulnerability assessment of highway bridges considering corrosion deterioration and repeated earthquake events. *Bull Earthq Eng*. 2019;17(3). doi:10.1007/s10518-018-0509-3
2. Rao AS, Lepech MD, Kiremidjian AS, Sun XY. Simplified structural deterioration model for reinforced concrete bridge piers under cyclic loading 1. In: *Life-Cycle of Structural Systems*. ; 2019. doi:10.1201/9781351204590-6
3. Shekhar S, Ghosh J, Padgett JE. Seismic life-cycle cost analysis of ageing highway bridges under chloride exposure conditions: modelling and recommendations. *Struct Infrastruct Eng*. 2018;14(7). doi:10.1080/15732479.2018.1437639
4. Kumar R, Gardoni P, Sanchez-Silva M. Effect of cumulative seismic damage and corrosion on the life-cycle cost of reinforced concrete bridges. *Earthq Eng Struct Dyn*. 2009;38(7). doi:10.1002/eqe.873
5. Kumar R, Gardoni P. Renewal theory-based life-cycle analysis of deteriorating engineering systems. *Struct Saf*. 2014;50. doi:10.1016/j.strusafe.2014.03.012
6. Ghosh J, Padgett JE. Probabilistic seismic loss assessment of aging bridges using a component-level cost estimation approach. *Earthq Eng Struct Dyn*. 2011;40(15). doi:10.1002/eqe.1114
7. Decò A, Frangopol DM. Life-cycle risk assessment of spatially distributed aging bridges under seismic and traffic hazards. *Earthq Spectra*. 2013;29(1). doi:10.1193/1.4000094
8. Titi A, Biondini F. On the accuracy of diffusion models for life-cycle assessment of concrete structures. *Struct Infrastruct Eng*. 2016;12(9). doi:10.1080/15732479.2015.1099110
9. Capacci L, Biondini F, Titi A. Lifetime seismic resilience of aging bridges and road networks. *Struct Infrastruct Eng*. 2020;16(2). doi:10.1080/15732479.2019.1653937
10. Capacci L, Biondini F. Probabilistic life-cycle seismic resilience assessment of aging bridge networks considering infrastructure upgrading. *Struct Infrastruct Eng*. 2020;16(4). doi:10.1080/15732479.2020.1716258
11. Moser RD, Hoeke L, Lisa J, Singh PM, Kahn LF, Kurtis KE. Corrosion of Steel Girder Bridge Anchor Bolts. *Transp Res Board 88th Annu Meet*. 2009;250(404).
12. Akiyama M, Frangopol DM, Matsuzaki H. Life-cycle reliability of RC bridge piers under seismic and airborne chloride hazards. *Earthq Eng Struct Dyn*. 2011;40(15). doi:10.1002/eqe.1108
13. Strauss A, Wendner R, Bergmeister K, Costa C. Numerically and Experimentally Based Reliability Assessment of a Concrete Bridge Subjected to Chloride-Induced Deterioration. *J Infrastruct Syst*. 2013;19(2). doi:10.1061/(asce)is.1943-555x.0000125
14. Fayaz J, Medalla M, Zareian F. Sensitivity of the response of Box-Girder Seat-type bridges to the duration of ground motions arising from crustal and subduction earthquakes. *Eng Struct*. 2020;219. doi:10.1016/j.engstruct.2020.110845
15. Fayaz J, Dabaghi M, Zareian F. Utilization of Site-Based Simulated Ground Motions for Hazard-Targeted Seismic Demand Estimation: Application for Ordinary Bridges in Southern California. *J Bridg Eng*. 2020;25(11). doi:10.1061/(asce)be.1943-5592.0001634
16. Caltrans. Caltrans Seismic Design Criteria Version 1.7. *Calif Dep Transp Sacramento, CA, US*. Published online 2013.
17. Kashani MM, Crewe AJ, Alexander NA. Nonlinear stress-strain behaviour of corrosion-damaged reinforcing bars including inelastic buckling. *Eng Struct*. 2013;48. doi:10.1016/j.engstruct.2012.09.034
18. Coronelli D, Gambarova P. Structural Assessment of Corroded Reinforced Concrete Beams: Modeling Guidelines. *J Struct Eng*. 2004;130(8). doi:10.1061/(asce)0733-9445(2004)130:8(1214)
19. Mander JB, Priestley MJN, Park R. Theoretical Stress-Strain Model for Confined Concrete. *J Struct Eng*. 1988;114(8). doi:10.1061/(asce)0733-9445(1988)114:8(1804)
20. Du YG, Clark LA, Chan AHC. Residual capacity of corroded reinforcing bars. *Mag Concr Res*. 2005;57(3). doi:10.1680/macr.2005.57.3.135

21. Biondini F, Vergani M. Deteriorating beam finite element for nonlinear analysis of concrete structures under corrosion. *Struct Infrastruct Eng*. 2015;11(4). doi:10.1080/15732479.2014.951863

22. Zhu M, McKenna F, Scott MH. OpenSeesPy: Python library for the OpenSees finite element framework. *SoftwareX*. 2018;7. doi:10.1016/j.softx.2017.10.009

23. Graves R, Jordan TH, Callaghan S, et al. CyberShake: A Physics-Based Seismic Hazard Model for Southern California. *Pure Appl Geophys*. 2011;168(3-4). doi:10.1007/s00024-010-0161-6

24. Azar S, Dabaghi M. Simulation-based seismic hazard assessment using monte-carlo earthquake catalogs: Application to cybershake. *Bull Seismol Soc Am*. 2021;111(3). doi:10.1785/0120200375

25. Boore DM. Orientation-independent, nongeometric-mean measures of seismic intensity from two horizontal components of motion. *Bull Seismol Soc Am*. 2010;100(4). doi:10.1785/0120090400

26. Deb A, Zha AL, Caamaño-Withall ZA, Conte JP, Restrepo JI. Updated probabilistic seismic performance assessment framework for ordinary standard bridges in California. *Earthq Eng Struct Dyn*. 2021;50(9). doi:10.1002/eqe.3459

27. Gentile R, Galasso C. Hysteretic energy-based state-dependent fragility for ground-motion sequences. *Earthq Eng Struct Dyn*. Published online 2020. doi:10.1002/eqe.3387